Research Article

# Dynamic Low-Pressure Measurement Using a Fiber Optic-based Fabry-Perot Interferometer

Pronnaruimon Talhakultorn and Saroj Pullteap*
Department of Mechanical Engineering, Faculty of Engineering and Industrial Technology, Silpakorn University, Nakhon Pathom, Thailand

* Corresponding author. E-mail: saroj@su.ac.th DOI: 10.14416/j.asep.2023.11.011
Received: 8 September 2023; Revised: 5 October 2023; Accepted: 25 October 2023; Published online: 28 November 2023


**Abstract**
A dynamic low-pressure measurement using a fiber optic-based Fabry-Perot Interferometer (FFPI) has been demonstrated in this work. The developed system has been divided into 2 main parts: pressure source and sensing system. The former is a chamber comprised of an elastic diaphragm, which proportionally deflects according to input pressure from an air pump. The FFPI, consequently, detects the material deflection and demodulates the parameter into useful pressure value via the fringe counting technique and Kirchhoff-Love's plate theory. To validate the performance of the developed system, a reference pressure instrument is utilized while the air pump feeds pressure of 0.34–6.57 mbar with 10 times repeatability into the system. The experimental results indicated that the FFPI can measure the pressure of 0.343–6.568 mbar, while the reference instrument showed the output values from 0.343–6.471 mbar, respectively. Moreover, the average and maximum percentage error in measurement is 1.27% and 2.67%, respectively. The resolution of the FFPI sensor is also analyzed to be approximately 0.05% or 0.0382 mbar/μm over all measurement ranges. Therefore, we conclude that the FFPI has high accuracy, resolution, linearity, and reliability in dynamic low-pressure measurements.

**Keywords**: Dynamic low-pressure measurement, Fabry-Perot interferometer, Fringe counting technique, Material deflection, Reference pressure instrument

## 1 Introduction

In modern industries, measuring instruments and sensors have become critical roles as integral components of automated control systems. However, it corresponds to the demand for user-friendly, high-precision equipment capable of autonomous decision-making. Furthermore, industrial machinery can benefit from the support of operating systems that are equipped with predefined datasets, thereby enhancing their operational speed. Consequently, a diverse array of sensors, encompassing categories such as pressure, temperature, chemical, and optical sensors, etc. [1] has found widespread adoption across a multitude of industries. Notably, pressure-sensing instruments are indispensable in a variety of contexts, including but not limited to the oil and gas sector, power plants, automotive manufacturing, and agriculture [2], [3]. Within the limitation of industrial processes, it becomes imperative to regulate, monitor, and sustain pressure levels in accordance with the specific requirements of each machine system [4]. In this context, low-pressure instruments can offer superior resolution and precision capabilities. Nonetheless, it is important to acknowledge that current devices possess certain limitations in their applications, most notably in terms of sensitivity, accuracy, precision, and high-precision or specialized pressure sensors can be expensive, which may be a limitation for budget-conscious applications [5].

Consequently, a fiber optic sensor (FOS) is another type of suitable pressure detector for low-pressure applications with several advantages over the

electronic commercial sensor such as high sensitivity, small size, immunity to electromagnetic waves, lightweight, and operational in noisy, hazardous, as well as narrow areas [6]–[10]. Several researchers have, therefore, investigated and developed low-pressure sensors using FOS. For instance, Riveraa *et al.*, [11] developed an extrinsic fiber Fabry-Perot interferometer (EFPI) based on thin polyester film using phase signal analysis at a variable pressure ranging from 0–2 psi. Results demonstrated that the EFPI had high efficiency with detection sensitivity close to 3.5 rad/psi. This study opens up a wide range of options for low-pressure detection. Moreover, Aime *et al.*, [12] developed a specific low-pressure sensor for aerodynamic applications. Two fiber optic strain sensing technologies based on fiber segment interferometry (FSI) and fiber Bragg grating (FBG) have been implemented. The pressure resolution was designed to be 23, 9.5, and 0.61 Pa, respectively. The results also showed that the pressure resolution of the FSI was 15 times greater than that of the FBG. In addition, Mishra *et al.*, [13] developed an optical pressure sensor based on the Fabry–Perot Interferometer (FPI) principle for a pressure range of 1 bar. A finite element (FE)-based sensor was also developed to simulate the structure and fluid element for the diaphragm and gas trapped in the cavity of a pressure sensor. The reference pressure and diaphragm deflection were assessed at different applied pressures. Analyzing the effects of gases trapped in the small sealed cavities of pressure sensors showed that the range of the diaphragm was more severely affected than sensors with smaller cavity lengths due to a greater change in reference pressure in the sealed compartment. However, the development of low-pressure instruments still has limitations. For example, measurement errors can occur in the sensing probe, and the pressure sensor is not able to measure the dynamic low-pressure range sufficiently [11].

In previous work, we preliminary developed an extrinsic fiber-based Fabry-Perot interferometer (EFFPI) for measuring the low-pressure in the range of 5–55 mbar with a maximum error of 3.77% [14]. However, we are continuing the development of a sensing system using the principle of the fiber optic-based Fabry-Perot interferometer (FFPI) for dynamic low-pressure measurement. The fringe counting technique cooperated with the material deformation theory is still utilized as a main technique to demodulate the obtained interference fringe to the pressure value. We anticipate that the development of pressure sensors for lower pressure measurements will yield increased sensitivity, but reduce responsiveness to the external incentives. Consequently, with the ability to accurately measure extremely low-pressure levels, these sensors can effectively mitigate the risks associated with pressures exceeding the system's capacity, thereby preventing potential accidents. Moreover, the reduced production costs associated with these sensors will enhance their affordability and accessibility to a broader user base. Furthermore, their user-friendly nature facilitates their integration into existing low-pressure detection systems, potentially enhancing their overall performance and reliability.

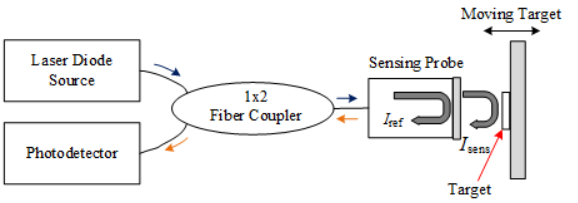


**Figure 1**: Basic structure of a FFPI.

## 2 Materials and Methods

The development of a dynamic low-pressure sensor using a fiber optic-based Fabry-Perot interferometer has been applied using the following theories and related studies.

### 2.1 *Fiber optic-based interferometers*

In general, the optical fiber-based interferometer has been classified into four main types; Mach-Zehnder, Michelson, Sagnac, and Fabry-Perot interferometers [15]. The fiber optic-based Fabry-Perot interferometer (FFPI) is one of the fiber optic interferometers that are widely applied as a detector for industrial applications, due to their several outstanding features such as high detection sensitivity, low cost, and simplicity of development [16]–[18]. The basic structure of this sensor is shown in Figure 1.

As shown in Figure 1, the basic structure of a fiber optic-based Fabry-Perot interferometer functions by using only a uniaxial element as a sensing arm, unlike

other interferometers that transmit signals from two axes (reference and sensing arms).The monochromatic light from the laser diode source is injected through a 1x2 fiber coupler and subsequently into the sensing arm. About 4% of the light is reflected at the fiber end as a reference signal ($I_{ref}$), while the rest is transmitted to the target and then reflected back to the sensing arm as a sensing signal ($I_{sens}$). Afterward, the two signals superimpose within the fiber arm, achieving an interference signal (I), which is modulated by a phase difference ($\phi$) [19]–[23], which can be determined by Equation (1):

$$I = I_{\text{sens}} + I_{\text{ref}} + 2\sqrt{I_{\text{sens}} I_{\text{ref}}}\cos\phi \tag{1}$$

In addition, the phase difference [20] between the sensing and reference signals can be expressed by Equation (2).

$$\phi = \frac{4\pi n \Delta l}{\lambda} \tag{2}$$

where. $n$ is the refrative index ($n$ = 1 when the medium is air), $\lambda$ is the wavelength of a monochromatic light source and $\Delta l$ is the cavity length variation

When the phase difference is perturbed, the output interference signal will be modulated, forming a set of cosinusoidal waveforms with each wave period corresponding to an interference fringe. Consequently, the number of interference fringe ($N$) can be applied to calculate the displacement ($D$) of a moving target, [24], [25], as shown in Equation (3).

$$D = N\frac{\lambda}{2} \tag{3}$$

### 2.2 *Deformation of material*

Material deformation is a process of changing the shape, appearance, and size of a material when forces such as pressure, tensile, compression, and shear are applied to it. However, such a process can be used to determine the thickness, resistance, stress, strain, and elastic modulus ($\delta$) of the material. The nature of the force acting on the material [26] in several ways can be demonstrated in Figure 2.

The determination of elastic modulus is a measure of the resistance of an elastic material before it reaches a critical point. This phenomenon can be determined

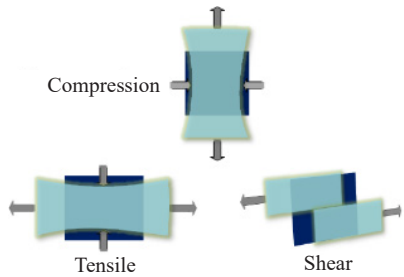


**Figure 2**: Nature of force acting on material.

from the relationship between the stress and strain of the material [27]–[29], as shown in Equation (4).

$$\delta = \frac{\sigma}{\varepsilon} \tag{4}$$

where: $\sigma$ is the stress of the material
ε is the strain of material

In addition, Poisson's ratio ($v$), which is the ratio of lateral strain to longitudinal strain [30], [31], can be expressed as Equation (5):

$$v = -\frac{\varepsilon_x}{\varepsilon_y} \tag{5}$$

where: $\varepsilon_x$ is the transverse strain of material
$\varepsilon_y$ is the axial strain of material

### 2.3 *Pressure measurement*

The relationship between the magnitude of the force acting perpendicularly to any area is pressure ($P$), as shown in Equation (6). The unit of pressure can be expressed in pascal (Pa), pound per square inch (Psi), or bar [32].

$$P = \frac{F}{A} \tag{6}$$

when: $F$ is the inducing force
$A$ is the area being acted upon

Pressure is also involved in several industrial applications [33]. Pressure measurement and control are, generally, required in the process of machine operations using qualified and sufficiently high-quality measuring instruments. As a result, most pressure-measuring devices are developed from optical devices [34], [35]. Optical pressure measuring devices usually rely on the deformation of a reflective material caused by induced pressure. Here, Kirchhoff-Love's plate

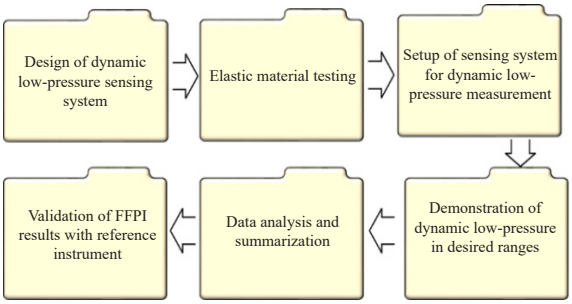


**Figure 3**: Workflow of dynamic low-pressure sensing development based on Fabry-Perot interferometer.

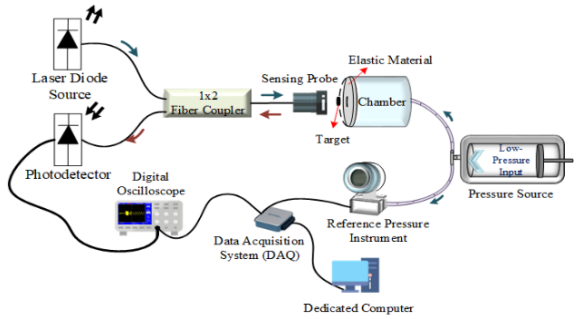


**Figure 4**: Structure of a dynamic low-pressure measurement using fiber optic-based Fabry-Perot interferometer.

theory for a clamped-edge circular diaphragm is demonstrated, which presents the relationship between the change in displacement and pressure as follows [36]–[41].

$$P = \frac{16\delta d^3 \Delta l}{3r^3(1-v^2)} \tag{7}$$

where: $d$ is the material thickness
$r$ is the deformation radius of the material
$\Delta l$ is the changes in displacement

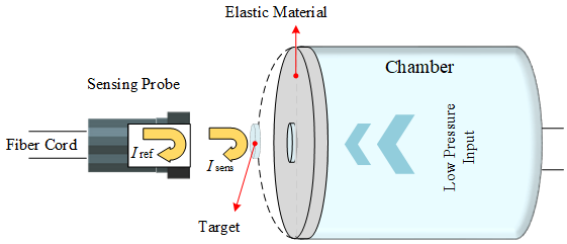


**Figure 5**: Concept of dynamic low-pressure measurement via changing of elastic material.

## 3 Experimental Setup

In this work, a low-pressure sensing system has been designed and implemented. The workflows of this system are illustrated in Figure 3.

The experiment is designed to collect the pressure values from a reference instrument ($P_{ref}$) and also the interference fringes from the developed system ($P_{FFPI}$), which was demonstrated at various pressure ranges for verifying the performance of the FFPI sensor. In addition, both pressure values obtained from Pref and PFFPI are next compared to determine the errors and the performance of the developed system.

### 3.1 *Dynamic low-pressure measurement using fiber optic-based Fabry-Perot interferometer*

As mentioned in the previous section, a dynamic low-pressure measurement using a fiber optic-based Fabry-Perot interferometer has been developed with its structure illustrated in Figure 4.

As shown in Figure 4, the dynamic low-pressure measurement system can be divided into 2 main parts: the dynamic low-pressure source and the fiber optic sensing system. The pressure source comprises an air pump that feeds in air pressure simultaneously to a chamber and a reference high-precision differential pressure instrument model: SITRANS P320 from Siemens. Note that the pressure instrument is applied as a pressure gauge during pressure feeding and also as a reference device for validating the developed FFPI. At the chamber, the feed-in pressure will induce upon an elastic material, proportionally deflecting it as illustrated in Figure 5.

As shown in Figure 5, the elastic material is deflected according to input pressure. This phenomenon can be detected by using an FFPI [31] and later demodulated into useful pressure readings via the fringe counting technique in Equation (7) [42]. To observe the output interference signal, a digital oscilloscope model: TDS2014B from Tektronix is utilized as a display. Meanwhile, a data acquisition unit simultaneously records the data from both the oscilloscope and reference pressure device for further analysis using MATLAB programming in a dedicated computer.


(a) (b)

**Figure 6**: Material testing process: (a) measuring of stress and strain in elastic material, (b) diameter measurement on material's fixation to chamber.

To validate the developed FFPI system, both the FFPI sensor and the reference instruments are exploited to measure input pressure. Here, the input pressure range is 0.343–6.417 mbar (measured by the reference device) and each selected value is performed in 10 times of repeatability. This experiment aims to verify the performance of the developed FFPI that is its accuracy, resolution, and linearity in low-pressure measurement.

### 3.2 *Elastic material testing process*

To apply the deformation theory for detecting the dynamic low-pressure using an optical fiber interferometer, the elastic material has been characterized for investigating its material thickness, Young's modulus ($E$), Poisson's ratio, and the radius, etc. An example of this investigation is depicted in Figure 6.

Figure 6 shows the measurement process of the elastic material by using a universal testing machine (UTM) *Model: 5969* from *Instron Engineering Corporation* for obtaining the stress, strain, and radius parameters. Consequently, the testing results are then used to calculate Young's modulus (or elastic modulus), and Poisson's ratio by using Equations (4) and (5), respectively. These parameters are summarized in Table 1.

**Table 1**: Elastic modulus, thickness, and Poisson's ratio of elastic material

| Description | Symbol | Values |
|---|---|---|
| Elastic modulus of material | $E$ | 6.365 MPa |
| Thickness of material | $h$ | 0.135 mm |
| Poisson's ratio of material | $v$ | 0.49 |
| Wavelength | $\lambda$ | 1311.82 nm |
| Bending radius | $r$ | 15 mm |

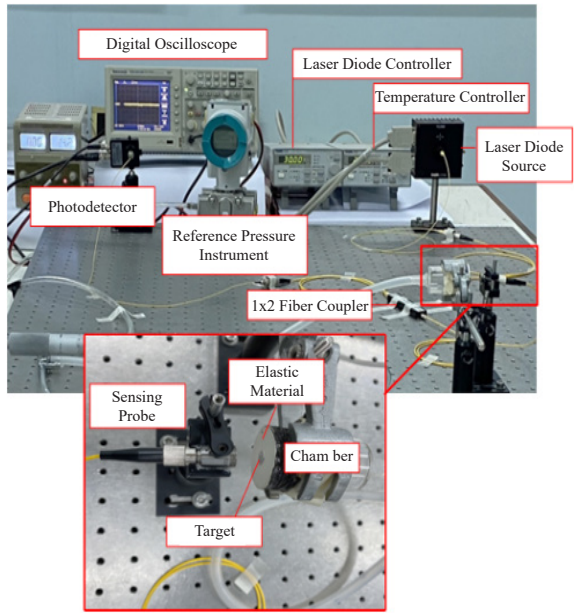


**Figure 7**: Experimental setup of a dynamic low-pressure measurement system using FFPI sensor.

## 4 Experimental Results and Discussion

As mentioned before, a fiber optic-based Fabry-Perot interferometer (FFPI) for dynamic low-pressure measurement has been developed in this research work. The experimental setup of the system is, therefore, shown in Figure 7.

As shown in Figure 7, the developed system is composed of 2 main parts, pressure source, and sensing system, respectively. Initially, when the whole system is installed without feeding any pressure, the output signal from the digital oscilloscope is displayed in Figure 8(a). On the other hand, when a dynamic pressure is fed into the system, the output signal plotted on the oscilloscope is presented in Figure 8(b). Moreover, this signal is next transferred to a dedicated computer and then demodulated using the MATLAB programming to calculate the output pressure. An example of the demodulated pressure has been plotted in Figure 8(c).

To validate the FFPI sensor's accuracy, pressure in the range of 0.34–6.417 mbar has been inducted into the system with 20 times repeatability for each test. The demodulated pressure obtained using the FFPI is then compared to that of the reference. Consequently, the experimental results are summarized in Table 2.

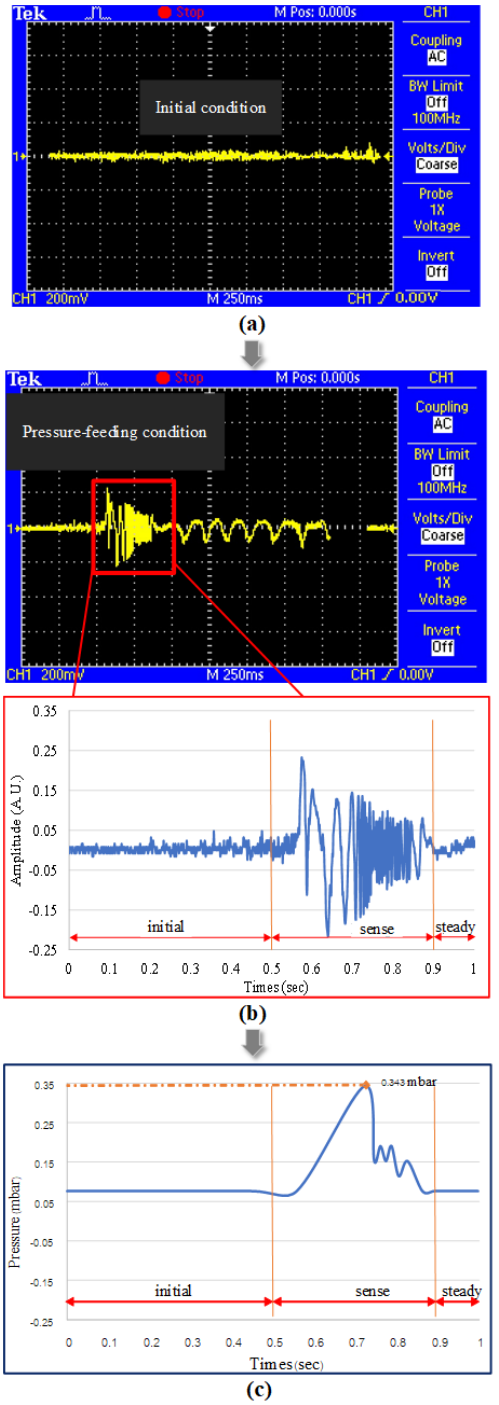


**Figure 8**: Output signal displayed on monitoring system: (a) at initial condition, (b) example of output interference fringes with pressure-feeding condition and (c) dynamic pressure plotted by MATLAB programming.

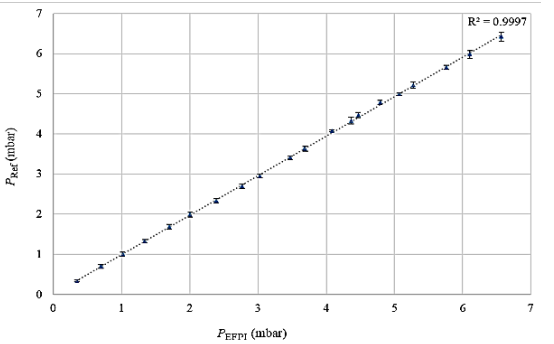


**Figure 9**: Relationship of output pressure obtained from FFPI vs. reference instrument.

**Table 2**: Experimental results from FFPI compared with reference pressure instrument

| Range | $P_{ref,\,Avg}$ (mbar) | $P_{FFPI,\,Avg}$ (mbar) | % ERROR |
|---|---|---|---|
| 1 | 0.343 | 0.343 | 0.00 |
| 2 | 0.694 | 0.697 | 0.43 |
| 3 | 1.003 | 1.013 | 0.99 |
| 4 | 1.330 | 1.341 | 0.82 |
| 5 | 1.682 | 1.699 | 1.00 |
| 6 | 1.987 | 2.004 | 0.85 |
| 7 | 2.331 | 2.389 | 2.43 |
| 8 | 2.697 | 2.766 | 2.49 |
| 9 | 2.948 | 3.029 | 2.67 |
| 10 | 3.410 | 3.471 | 1.76 |
| 11 | 3.628 | 3.691 | 1.71 |
| 12 | 4.080 | 4.084 | 0.10 |
| 13 | 4.332 | 4.366 | 0.78 |
| 14 | 4.470 | 4.469 | 0.02 |
| 15 | 4.778 | 4.789 | 0.23 |
| 16 | 4.988 | 5.071 | 1.64 |
| 17 | 5.212 | 5.273 | 1.16 |
| 18 | 5.657 | 5.760 | 1.79 |
| 19 | 5.975 | 6.107 | 2.16 |
| 20 | 6.417 | 6.568 | 2.30 |

The results in Table 2 show that the maximum percentage error of the developed FFPI is 2.67%, while the average percentage error is 1.27%, respectively. In addition, the relationship between the pressure output obtained from the reference instrument versus the FFPI sensor has been plotted in Figure 9. This relation has investigated the linearity of the FFPI for dynamic low-pressure measurements compared with the standard value.

Figure 9 shows the relationship between

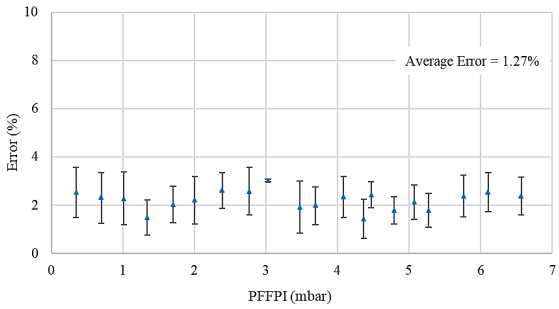


**Figure 10**: Measurement error obtained from FFPI.

the output low-pressures obtained from the reference pressure instrument ($P_{ref}$) and the fiber optic-based Fabry-Perot interferometer ($P_{FFPI}$) for each dynamic pressure range (each averaged from 10 times repeatable tests). A linear correlation analysis indicates a coefficient of determination ($R^2$) of 0.9997. This implies that the FFPI pressure sensor has very high linearity. Moreover, the percentage measurement error from the experiment has been illustrated in Figure 10.

Figure 10 depicts the relationship between the output low-pressure range achieved from the FFPI sensor and the percentage error of each pressure range. The result indicates that a maximum percentage error is found to be 2.67% at the pressure range of 2.948 mbar, while the average error over all pressure ranges is 1.27%, respectively. Thus, 3 main factors causing the error can be deduced: the surrounding environment affecting the elastic material, the pressure leak from the source and chamber, and the improper sensor installation. Nevertheless, the experimental results verified that the FFPI sensor has the capability for dynamic low-pressure measurement with high linearity ($R^2$ value equals to 0.9997), and also a high resolution of approximately 0.05% or 0.0382 mbar/m.

## 4 Conclusions

In this work, a dynamic low-pressure sensing system using a fiber optic-based Fabry-Perot interferometer (FFPI) has been developed. The interference fringe counting technique is applied in conjunction with the material deflection theory to calculate the desired low pressure. Furthermore, a reference pressure instrument is simultaneously operated to determine the performance of the developed FFPI system. In the experiment, air pressure input into the system ranges from 0.34–6.57 mbar, and the testing also are performed for 10 times of repeatability. The experimental results indicate that the FFPI can measure the pressure in the range of 0.343–6.568 mbar, while the reference pressure instrument measures in the range of 0.343–6.417 mbar. Further, a maximum percentage error was found to be 2.67%, while an average percentage error was 1.27%, respectively. In this study, a total of 20 distinct pressure ranges were subjected to testing, spanning from 0.343–6.417 microbars. Upon examining the average values of FFPI within each of these pressure ranges, it becomes evident that certain pressure intervals exhibit a notably frequent occurrence. This observation underscores the remarkable sensitivity achieved by the developed detector, a fact that is highly commendable from the perspective of the authors. The experiment results demonstrate the high efficiency and high resolution of the low-pressure measurement. Therefore, it can be further developed as a cost-effective measuring instrument. Moreover, it could be conceivable in the future to develop a low-pressure measuring instrument for industrial applications in Thailand.

## Acknowledgment

This research has received funding and support from Silpakorn University Research, Innovation, and Creative Fund.

## Author Contributions

S.P. Conceptualization; S.P. and P.T.: methodology; S.P. and P.T.: validation; P.T. and S.P.: formal analysis; P.T. and S.P.: resources; P.T. and S.P.: writing-original draft preparation; P.T. and S.P.: writing-review and editing; S.P., supervision; All authors have read and agreed to the published version of the manuscript.

## Conflicts of Interest

The authors declare no conflict of interest.

## References

[1] M. A. Kotov, P.V. Kozlov, G. Ya Gerasimov, V. Y. Levashov, A. N. Shemyakin, N. G. Solovyov, M. Y. Yakimov, V. N. Glebov, G. A. Dubrova, and A. M. Malyutin, “Thermoelectric detector

application for measuring the ignition delay time in a shock heated combustible mixture," *Acta Astronautica*, vol. 204, pp. 787–793, 2023.

[2] K. Chimklin and C. Chungchoo, "Optimization of design for air gap sensor using the response surface methodology," *Applied Science and Engineering Progress*, vol. 16, no. 1, 2023, Art. no. 5687, doi: 10.14416/j.asep.2022.01.003.

[3] I. Floris, J. M. Adam, P. A. Calderón, and S. Sales, "Fiber optic shape sensors: A comprehensive review," *Optics and Lasers in Engineering*, vol. 139, 2021, Art. no. 106508.

[4] C. Li, J. Xie, F. Cordovilla, J. Zhou, R. Jagdheesh, and J. L. Ocaña, "Design fabrication and characterization of an annularly grooved membrane combined with rood beam piezoresistive pressure sensor for low-pressure measurements," *Sensors and Actuators A: Physical*, vol. 279, pp. 525–536, 2018.

[5] E. Vorathin, Z. M. Hafizi, N. Ismail, and M. Loman, "Review of high sensitivity fiber-optic pressure sensors for low pressure sensing," *Optics & Laser Technology*, vol. 121, 2020, Art. no. 105841.

[6] D. D. Vo, R. Moradi, M. B. Gerdroodbary, and D.D. Ganji, "Measurement of low-pressure Knudsen force with deflection approximation for gas detection," *Results in Physics*, vol. 13, 2019, Art. no.102257.

[7] P. Thaisongkroh and S. Pullteap, "Investigation of fiber optic-based-refractometer for biogas sensing,"*Applied Science and Engineering Progress*, vol.16, no.4, 2023, Art. no. 6793, doi: 10.14416/j.asep.2023.03.003.

[8] J. Jiang, T. Zhang, S. Wang, K. Liu, C. Li, Z. Zhao, and T. Liu, "Noncontact ultrasonic detection in low-pressure carbon dioxide medium using high sensitivity fiber-optic fabry-peot sensor system," *Journal of Lightwave Technology*, vol. 35, no. 23, pp. 5079–5085, 2017.

[9] H. Liao, P. Lu, L. Liu, S. Wang, W. Ni, X. Fu, D. Liu, and J. Zhang, "Phase demodulation of Short-Cavity Fabry-Perot interferometric acoustic sensors with two," *IEEE Photonics Journal*, vol. 9, no. 2, 2017, Art no. 7102207, doi: 10.1109/JPHOT.2017.2689771.

[10] S. Pullteap, H.-C. Seat, and T. M. Bosch, "Modified fringe-counting technique applied to a dual-cavity fiber Fabry-Pérot vibrometer," *Optical Engineering*, vol. 46, no. 11, 2017, Art. no. 115603.

[11] M. Gutierrez-Rivera, D. Jauregui-Vazquez, J. M. SierraHernandez, D. F. Garcia-Minac, Y. Lopez-Dieguez, J. M. Estudillo-Ayala, and R. Rojas-Laguna, "Low-pressure fiber-optic sensor by polyester Fabry-Perot cavity and its phase signal processing analysis," *Sensors and Actuators A: Physical*, vol. 315, 2020, Art. no. 112338.

[12] L. F. J. Aime, T. Kissinger, S. W. James, E. Chehura, A. Verzeletti, and R. P. Tatam, "High sensitivity pressure measurement using optical fibre sensors mounted on a composite diaphragm," *Optics Express*, vol. 29, no. 3, 2021.

[13] S. Mishra, R. Balasubramaniam, and S. Chandra, "Finite element analysis and experimental validation of suppression of span in optical MEMS pressure sensor," *Microsystem Technologies*, vol. 25, pp. 3691–3701, 2019.

[14] P. Thaisongkroh, S. Pullteap, and H. C. Seat, "Low-pressure measurement using an extrinsic fiber based Fabry-Perot interferometer for industrial applications," *Engineering Journal*, vol. 25, no. 2, pp. 317–325, 2020.

[15] G. A. Lashari, F. Mumtaz, Z. Ai, and Y. Dai, "Recent advancements and future challenges in hybrid optical fiber interferometers," *Optik*, vol. 282, 2023, Art. no. 170860.

[16] C.-B. Yu, Y. Wu, C. Li, F. Wu, J.-H. Zhou, Y. Gong, Y.-J. Rao, and Y.-F. Chen, "Highly sensitive and selective fiber-optic Fabry-Perot volatile organic compounds sensor based on a PMMA film," *Optical Materials Express*, vol. 7, no. 6, pp. 2111–2116, 2017.

[17] M. I. Reja, L. V. Nguyen, H. Ebendorff-Heidepriem, and S. C. Warren-Smith, "Multipoint pressure sensing at up to 900 ºC using a fiber optic multimode interferometer," *Optical Fiber Technology*, vol. 75, Jan. 2023, Art. no. 103157.

[18] Y. Cao, L. Wang, Z. Lu, G. Wang, X. Wang, Y. Ran, X. Feng, and B.-O. Guan, "High-speed refractive index sensing system based on Fourier domain mode-locked laser," *Optics Express*, vol. 27, no. 6, pp. 7988–7996, 2019.

[19] M. Elsherif, A. E. Salih, M. Elsherif, A. E. Salih, M. G. Muñoz, F. Alam, B. AlQattan, D. S. Antonysamy, M. F. Zaki, A. K. Yetisen, S. Park, T. D. Wilkinson,

and H. Butt, "Optical fiber sensors: Working principle, applications, and limitations," *Advances in Photonics Research*, vol. 3, no. 11, 2022, Art. no. 2100371.

[20] B. Yang, J. Zhang, Y. Yin, Y. Niu, and M. Ding, "A sensing peak identification method for fiber extrinsic fabry-perot interferometric refractive index sensing," *Sensors*, vol. 19, no. 1, 2019, Art. no. 96.

[21] Q. Zhang, J. Lei, Y. Chen, Y. Wu, C. Chen, and H. Xiao, "3D printing of all-glass fiber-optic pressure sensor for high temperature applications," *IEEE Sensors Journal*, vol. 23, 2019, Art. no. 11242.

[22] H. Chen, J. Liu, X. Zhang, W. Wang, Z. Ma, W. Lv, and Z. Guo, "High-order harmonic-frequency cross-correlation algorithm for absolute cavity length interrogation of white-light fiber-optic Fabry-Perot sensors," *Journal of Lightwave Technology*, vol. 38, no. 4, pp. 953–960, 2020.

[23] D. Pawar and S. N. Kale, "A review on nanomaterial-modified optical fiber sensors for gases, vapors, and ions," *Microchimica* Acta, vol. 186, p. 253, 2019.

[24] Y. Zhou, Z. Dongjian, C. Zhuoyan, and L. Yongtao, "Research on a novel inclinometer based on distributed optical fiber strain and conjugate beam method," *Measurement*, vol. 153, Mar. 2020, Art. no. 107404.

[25] C. Xiong, W. Wan, J. Chen, D. Zeng, and M. Cai, "Fast high-precision displacement measurement system based on fringe image analysis techniques," *Results in Physics*, vol. 17, 2020, Art. no. 103048.

[26] J. Liu, Z. Su, Y. Wang, J. He, Z. Liu, H. Wang, Y. Tian, and W. Yang, "Approaching diamond's theoretical elasticity and strength limits," *Nature Communications*, vol. 10, 2019, Art. no. 5533.

[27] R. Khan and Z. Mustansar, "Reliability of using elastic modulus for non-homogeneous materials," *MATEC Web of Conferences*, vol. 49, 2016, Art. no. 109001.

[28] C. Uff, L. Garcia, J. Fromageau, A. Chakraborty, N. Dorward, and J. Bamber, "Further characterization of changes in axial strain elastograms due to the presence of slippery tumor boundaries," *Journal of Medical Imaging*, vol. 5, no. 2, 2018, Art. no. 021211.

[29] A. Yodrux, N. Yodpijit, and M. Jongprasithpornt, "Stress and displacement analysis of dental implant threads using three-dimensional finite element analysis," *Applied Science and Engineering Progress*, vol. 12, no. 3, pp. 216–222, 2019, doi: 10.14416/j.ijast.2018.09.002.

[30] JTG D50-2017, "Specifications for Design of Highway Asphalt Pavement," Ministry of Transport of the People's Republic of China, Beijing, 2017.

[31] H. Belyadi, E. Fathi, and F. Belyadi, "Rock mechanical properties and in situ stresses" in *Hydraulic Fracturing in Unconventional Reservoirs*, 2nd ed., Texas: Gulf Professional Publishing, pp. 215–231, 2019.

[32] S. Ronen, "Psi, pascal, bars, and decibels," *The Leading Edge*, vol. 21, no. 1, 2002, doi: 10.1190/1.1487322.

[33] M. Liu, Q. Cai, and H. Song, "Regional strain homogenized diaphragm based FBG high pressure sensor," *Sensors and Actuators A: Physical*, vol. 355, Jun. 2023, Art. no. 114298.

[34] P. Song, Z. Ma, J. Ma, L. Yang, J. Wei, Y. Zhao, M. Zhang, F. Yang, and X. Wang, "Recent progress of miniature MEMS pressure sensors," *Micromachines*, vol. 11, no. 1, 2020, Art. no. 56.

[35] K. M. Fadeev, D. D. Larionov, L. A. Zhikina, A. M. Minkin, and D. I. Shevtsov, "A fiber-optic sensor for simultaneous temperature and pressure measurements based on a Fabry–Perot interferometer and a fiber bragg grating," *Instruments and Experimental Techniques*, vol. 63, pp. 543–546, 2020.

[36] B. Xu, Y. Liu, D. Wang, D. Jia, and C. Jiang, "Optical fiber Fabry–Perot interferometer based on an air cavity for gas pressure sensing," *Photonics Research*, vol. 9, no. 2, 2017, Art. no. 7102309.

[37] M. Li, M. Wang, and H. Li, "Optical MEMS pressure sensor based on Fabry-Perot interferometry," *Optics Express*, vol. 14, pp. 1497–1504, 2016.

[38] Y. Zhou and K. Huang, "On simplified deformation gradient theory of modified gradient elastic Kirchhoff–Love plate," *European Journal of Mechanics/A Solids*, vol. 100, Art. no. 105014, 2023.

[39] M. W. Witczak and M. W. Mirza, "Development of relationships to predict Poisson's ratio for paving materials," Inter team Technical Report

for NCHRP 1–37A University of Maryland, College Park, Maryland, USA, 1999.

[40] Y. Javed, M. Mansoor, and I. A. Shah, "A review of principles of MEMS pressure sensing with its aerospace applications," *Sensor Review*, vol. 39, no. 5, pp. 652–664, 2019.

[41] D. Jauregui-Vazquez, M. E. Gutierrez-Rivera, D. F. Garcia-Mina, J. M. Sierra-Hernandez, E. Gallegos-Arellano, J. M. Estudillo-Ayala, J. C. Hernandez-Garcia, and R. Rojas-Laguna, "Low pressure and liquid level fber-optic sensor based on polymeric Fabry–Perot cavity," *Optical and Quantum Electronics*, vol. 53, 2021, Art. no. 237.

[42] Z. Xinlei, Y. Qingxu, and P. Wei, "Fiber-optic Fabry-Perot pressure sensor for down-hole application," *Optics and Lasers in Engineering*, vol. 121, pp. 289–299, 2019.